Synthesis, Molecular Modeling Studies, and Pharmacological Activity of Selective A₁ Receptor Antagonists

Francesco Bondavalli,[†] Maurizio Botta,*,[‡] Olga Bruno,[†] Andrea Ciacci,[‡] Federico Corelli,[‡] Paola Fossa,*,[†] Antonio Lucacchini,[§] Fabrizio Manetti,[‡] Claudia Martini,[§] Giulia Menozzi,[†] Luisa Mosti,[†] Angelo Ranise,[†] Silvia Schenone,[†] Andrea Tafi,[‡] and Maria Letizia Trincavelli[§]

Dipartimento di Scienze Farmaceutiche, Università degli Studi di Genova, Viale Benedetto XV n.3, I-16132 Genova, Italy, Dipartimento Farmaco Chimico Tecnologico, Università degli Studi di Siena, Via Aldo Moro, I-53100 Siena, Italy, and Dipartimento di Psichiatria, Neurobiologia, Farmacologia e Biotecnologie, Università degli Studi di Pisa, Via Bonanno, I-56126, Italy

Received June 10, 2002

We present a combined computational study aimed at identifying the three-dimensional structural properties required for different classes of compounds to show antagonistic activity toward the A₁ adenosine receptor (AR). Particularly, an approach combining pharmacophore mapping, molecular alignment, and pseudoreceptor generation was applied to derive a hypothesis of the interaction pathway between a set of A₁ AR antagonists taken from the literature and a model of the putative A₁ receptor. The pharmacophore model consists of seven features and represents an improvement of the N^6-C8 model, generally reported as the most probable pharmacophore model for A₁ AR agonists and antagonists. It was used to build up a pseudoreceptor model able to rationalize the relationships between structural properties and biological data of, and external to, the training set. In fact, to further assess its statistical significance and predictive power, the pseudoreceptor was employed to predict the free energy of binding associated with compounds constituting a test set. While part of these molecules was also taken from the literature, the remaining compounds were designed and synthesized by our research group. All of the new compounds were tested for their affinity toward A₁, A₂ₐ, and A₃ AR, showing interesting antagonistic activity and A₁ selectivity.

Introduction

Adenosine is a ubiquitous neuromodulator in both the periphery and the central nervous system (CNS). The effects elicited by adenosine are mediated by its interactions with four receptor subtypes termed A₁, A₂ₐ, A₂ᵦ, and A₃, which can be distinguished pharmacologically,[1] based on the rank order of potency of agonists and antagonists.[2] These receptors belong to the superfamily of G-protein-coupled receptors and contain seven transmembrane domains (α-helices), interconnecting loops, an extracellular terminal amino residue, and a cytoplasmic terminal carboxylate residue.[3] Adenosine receptors (ARs) from different species show a very high amino acid sequence homology (82−93%), with the only exception of the A₃ subtype, which exhibits a 74% primary sequence homology between rat and human or sheep.[4]

The physiological significance and function of endogenous adenosine have been extensively researched. Adenosine has been described as a neuromodulator in the CNS, possessing global importance in the modulation of the molecular mechanisms underlying many aspects of brain function by mediating central inhibitory effects. The development of agonists for the adenosine A₁ receptor able to mimic the central inhibitory effects of adenosine (and so inhibiting neurotransmitter re-

lease) may therefore be clinically useful as neuroprotective agents. On the contrary, adenosine antagonists (such as the alkylxanthines) stimulate the activity of the CNS and have proven to be effective as cognition enhancers. This is the joint action of antagonism of the sedative effects caused by adenosine and of increasing cerebral blood flow, thus increasing glucose and oxygen availability to the brain.

In the last two decades, many efforts have been invested in the synthesis of selective AR ligands for their potential therapeutic use. This research has resulted in the synthesis of a number of AR agonists and antagonists.[5,6] Particularly, selective AR subtype antagonists are sought as antiinflammatory, antiasthmatic, and antiischemic agents.[7,8]

In addition, A₁ selective antagonists may have therapeutic potential in the treatment of various forms of dementia, for example, in Alzheimer's[6] and Parkinson's[9] disease. Some compounds have been developed as kidney protective diuretics and for the treatment of asthma and depression.[10] Moreover, on the basis of the fact that adenosine plays a role in mediating the haemodynamic changes associated with acute renal failure, compounds that antagonize the renal effects of adenosine are potential renal protective agents.[11,12] As an example, the antagonist 1,3-dipropyl-8-(3-noradamantyl)xanthine **13** is currently undergoing clinical trials as a renal protective agent.[13]

The first AR antagonists reported were the natural xanthines, caffeine and theophylline, but potent and selective antagonists have stemmed from multiple

* To whom correspondence should be addressed. M.B.: Tel: +39 0577 234306. Fax: +39 0577 234333. E-mail: botta@unisi.it. P.F.: Tel: +39 010 3538361. Fax: +30 010 3538358. E-mail: fossap@unige.it.
† Università degli Studi di Genova.
‡ Università degli Studi di Siena.
§ Università degli Studi di Pisa.

1a: R = Me, R$_1$ = *n*-But
1b: R = H, R$_1$ = N=C(CH$_3$)$_2$
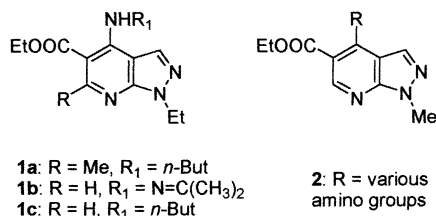**1c**: R = H, R$_1$ = *n*-But

2: R = various amino groups

Figure 1.

substitution of the parent heterocycle. On the other hand, many structurally different nonxanthine derivatives have been synthesized and studied as A$_1$ AR and A$_2$ AR antagonists. Comparison of compounds belonging to different classes of antagonists highlighted that despite being structurally diverse, most of the known ligands show some common features. In general, the structures are planar, aromatic, or π-electron rich and nitrogen-containing heterocycles. The heterocycles are most often 6:5 fused bicycles or 6:6:5 fused tricycles, substituted with hydrophobic moieties. Additionally, antagonists lack the ribose moiety, which is essential for agonist activity.

Important classes of A$_1$ selective antagonists are the prototypic xanthine derivatives (preferably with bulky cycloalkyl substituent at the C8-position), adenine derivatives including aza and deaza analogues of adenine, and other various heterocyclic compounds such as pyrrolo-pyrimidines and pyrimido-indoles.[14,15] Moreover, some literature reports revealed that the pyrazolo-[3,4-*b*]pyridine scaffold provides compounds that effectively bind A$_1$ AR.

As an example, tracazolate **1a**, etazolate **1b**, and cartazolate **1c** (Figure 1) are among the first nonxanthine antagonists reported in the literature,[16] compound **1c** being the most potent and quite selective antagonist even more potent than theophylline at both A$_1$ and A$_2$ AR. They were also found to inhibit binding at A$_1$ adenosine brain receptors.[17,18] An additional example is represented by a series of (substituted)-4-aminopyrazolo[3,4-*b*]pyridines **2**[19] (Figure 1), showing interesting affinity for A$_1$ and A$_2$ receptors with the most active compound possessing affinity of 0.3 and 0.5 μM for A$_1$ and A$_{2a}$ AR, respectively, without selective antagonist activity. Finally, many other products with similar activity have been recently patented.[20]

On the basis of this experimental evidence, within our research project on A$_1$ AR antagonists, we have recently designed new pyrazolo[3,4-*b*]pyridine derivatives[21] with the aim of obtaining compounds possibly characterized by high affinity and selectivity toward the A$_1$ AR. In detail, a long lipophilic chain with an aromatic moiety (chloroalkylphenyl, chloroalkylphenoxy, and styryl) has been placed at the 1-position of the bicyclic nucleus, instead of both the small methyl and the ethyl groups previously reported (see compounds **1** and **2**). Moreover, various alkylamino, arylamino, and cycloalkylamino moieties with different length and bulkiness, as well as heterocyclic substituents with sizes variable from five to seven members in the ring, have been added to the 4-position of the scaffold with the purpose of exploring steric and electronic properties that a group in this position should have to improve affinity toward A$_1$ AR. Synthetic pathways and biological data of the new

pyrazolo-pyridines **10**−**12** have been reported in Scheme 1 and Table 1.

Finally, a two step computational protocol has been applied to build a pharmacophore model for A$_1$ AR antagonists and a pseudoreceptor model of the A$_1$ AR. The latter model, able to rationalize the relationships between the chemical features of A$_1$ AR antagonists and their binding affinity data, shows a good statistical significance (correlation coefficient, $r = 0.9$; rms deviation, rmsd = 0.6 kcal/mol) and successfully estimates the affinities of the molecules of, and external to, the training set.

Chemistry

Scheme 1 reports the synthesis of the new compounds **10**−**12**. 2-Hydrazino-1-phenylethanol **3a**, prepared according to a literature procedure,[22] reacted with ethylethoxymethylene-cyanoacetate **4** in anhydrous toluene to give 5-amino-1-(2-hydroxy-2-phenylethyl)-1*H*-pyrazole-4-carboxylic acid ethyl ester **5a** in a very good yield (80%). Basic hydrolysis (EtOH/NaOH) of **5a** led to the carboxy intermediate **6a**, which by thermal decarboxylation at 185 °C[19] quantitatively afforded 2-(5-aminopyrazol-1-yl)-1-phenylethanol **7a**.

Condensation of **7a** with diethyl ethoxymethylenemalonate gave the intermediate **8a**, which upon treatment with POCl$_3$ at reflux (36 h) underwent the cyclization to the pyrazolo-pyridine nucleus with a concurrent chlorination of the hydroxy side chain. Chromatographic purification with Florisil and CHCl$_3$ as the eluant gave **9a** in a 60% overall yield.

The same reaction sequence was applied to **3b** to afford **9b** with a 40% yield in the last step, probably because of a partial hydrolysis involving the phenoxy substituent. Regioselective substitution of the C4 chlorine of compounds **9** with an excess of various amines (method A, Experimental Section) afforded the desired products **10a**−**n** and **11a**−**h** in good yield (Table 1). Compounds **12a**−**i** have been obtained in a 70−90% yield (Table 1) by treating **10a**−**c**,**e**−**g**,**j**−**l** with an excess of 1,8-diazabicyclo[5.4.0]undec-7-ene (DBU) at 80 °C (method B, Experimental Section).

It is interesting to point out that the chlorine atom at the side chain of all of the new compounds has never been substituted by the amino group. This hypothesis was proved by the ^{1}H NMR chemical shifts of the CH$_2$-CH side chain protons, which gave an ABX complex pattern owing to their nonequivalence and by the subsequent dehydrochlorination with DBU to give the corresponding styryl derivatives.

Biology

Compounds were tested for their ability to displace [^{3}H]-N^6-cyclohexyladenosine (CHA) on A$_1$ AR in bovine cortical membranes, [^{3}H]-2-{[4-(2-carboxyethyl)phenethyl]amino}-5′-(*N*-ethylcarbamoyl)adenosine (CGS21680) on A$_{2a}$ AR in bovine striatal membranes, and [^{125}I]-N^6-(3-iodo-4-aminobenzyl)-5′-*N*-methylcarboxamidoadenosine (AB-MECA) to A$_3$ AR in bovine cortical membranes, following a reported procedure.[23] The A$_1$, A$_{2a}$, and A$_3$ receptor binding affinities, expressed as K_i or percent of binding for compounds **10**−**12**, are reported in Table 2.

Scheme 1[a]
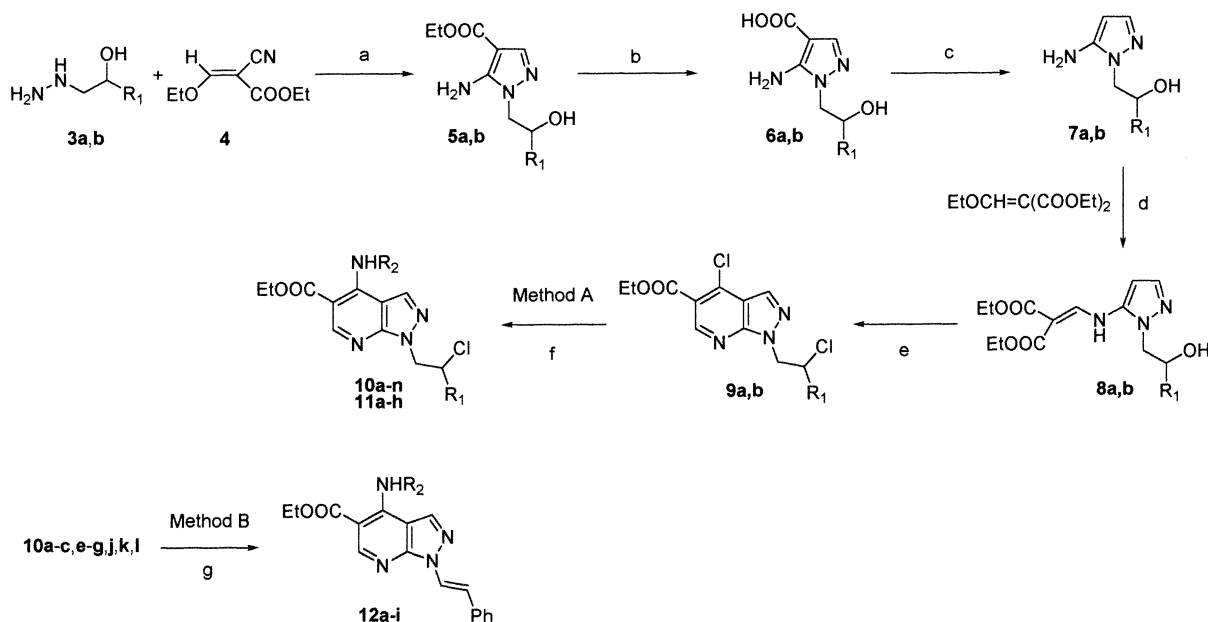
[a] Compounds: **3a**, R_1 = Ph; **3b**, R_1 = CH$_2$OPh; **5a**, R_1 = Ph; **5b**, R_1 = CH$_2$OPh; **6a**, R_1 = Ph; **6b**, R_1 = CH$_2$OPh; **7a**, R_1 = Ph; **7b**, R_1 = CH$_2$OPh; **8a**, R_1 = Ph; **8b**, R_1 = CH$_2$OPh; **9a**, R_1 = Ph; **9b**, R_1 = CH$_2$OPh; **10a**, R_1 = Ph, R_2 = NH*n*-Pr; **10b**, R_1 = Ph, R_2 = NHcyclopropyl; **10c**, R_1 = Ph, R_2 = NH*n*-Bu; **10d**, R_1 = Ph, R_2 = NH*t*-Bu; **10e**, R_1 = Ph, R_2 = NHCH$_2$CH$_2$OEt; **10f**, R_1 = Ph, R_2 = NHcyclohexyl; **10g**, R_1 = Ph, R_2 = 1-pyrrolidinyl; **10h**, R_1 = Ph, R_2 = 4-morpholinyl; **10i**, R_1 = Ph, R_2 = NHPh; **10j**, R_1 = Ph, R_2 = NHCH$_2$Ph; **10k**, R_1 = Ph, R_2 = NHCH$_2$CH$_2$OPh; **10l**, R_1 = Ph, R_2 = 1-piperidinyl; **10m**, R_1 = Ph, R_2 = 1-hexahydroazepinyl; **10n**, R_1 = Ph, R_2 = 1-(4-methyl)piperazinyl; **11a**, R_1 = CH$_2$OPh, R_2 = NHcyclopropyl; **11b**, R_1 = CH$_2$OPh, R_2 = NH*n*-Bu; **11c**, R_1 = CH$_2$OPh, R_2 = NHCH$_2$CH$_2$OEt; **11d**, R_1 = CH$_2$OPh, R_2 = NHcyclohexyl; **11e**, R_1 = CH$_2$OPh, R_2 = 1-pyrrolidinyl; **11f**, R_1 = CH$_2$OPh, R_2 = 4-morpholinyl; **11g**, R_1 = CH$_2$OPh, R_2 = NHCH$_2$Ph; **11h**, R_1 = CH$_2$OPh, R_2 = NHCH$_2$Ph; **12a**, R_2 = NH*n*-Pr; **12b**, R_2 = NHcyclopropyl; **12c**, R_2 = NH*n*-Bu; **12d**, R_2 = NHCH$_2$CH$_2$OEt; **12e**, R_2 = NHcyclohexyl; **12f**, R_2 = 1-pyrrolidinyl; **12g**, R_2 = 4-morpholinyl; **12h**, R_2 = NHCH$_2$Ph, **12i**, R_2 = NHCH$_2$CH$_2$Ph. Reagents: (a) anhydrous toluene; (b) EtOH, NaOH; (c) 185 °C, HCl 6N; (d) 120 °C, Et$_2$O; (e) POCl$_3$, reflux; (f) anhydrous toluene, NHR$_2$; (g) DBU, absolute EtOH.

Moreover, to determine the intrinsic activity of **10g**,**k**, found to be the most active compounds toward A$_1$ ARs, competition studies were performed in the presence and in the absence of 1 mM guanosine 5′-triphosphate (GTP) using the radiolabeled antagonist [^{3}H]DPCPX. The GTP shift is an in vitro parameter often indicative of intrinsic activity. GTP shift represented the ratio between the compound affinity constant in the presence and in the absence of GTP. GTP modulates the affinity of agonist compound whereas it does not affect the affinity for an antagonist compound. A GTP shift value >1 is indicative of an agonist profile; a GTP shift near to 1 is indicative of an antagonist profile. In Table 3, the GTP shift values of the selected compounds and R-PIA, included as standard, were reported. At the A$_1$ ARs, the selected compounds displayed no significant GTP shift, suggesting that they elicited an antagonist profile. In contrast, the standard agonist R-PIA exhibited a larger GTP shift value of 4.7. Intrinsic activity of compounds **10g**,**k** was also assessed by adenylyl cyclase functional assay evaluating their ability to reverse the inhibition of forskolin-stimulated adenylyl cyclase activity induced by the agonist CHA (100 nM). In rat cerebral cortex membranes, the A$_1$ adenosine agonist CHA induced a maximal inhibition of adenylyl cyclase activity of 15–20% of total activity, under conditions of stimulation (typically 3–4-fold) in the presence of 0.1 mM forskolin, with an IC$_{50}$ value of 1.4 ± 7 nM.[24] The inhibiton effect of CHA (100 nM) on adenylyl cyclase activity was antagonized completely and in a concentration-dependent manner by derivatives **10g**,**k** with an IC$_{50}$ value of 153.7 ± 9.8 nM and 52.2 ± 3.3 nM, respectively

2). The affinity constant values of compounds **10g**,**k** were also determined on rat cerebral cortex with results similar to those obtained from bovine tissues. In fact, while **10g** possessed an affinity of 140 nM toward rat A$_1$ AR vs a value of 98 nM toward bovine A$_1$ AR, **10k** showed an affinity of 73 nM toward rat A$_1$ AR vs a value of 50 nM toward bovine A$_1$ AR.

Structure−Activity Relationship Considerations on the New Compounds. Table 1 reports the A$_1$, A$_{2a}$, and A$_3$ AR binding affinities, expressed as K_i or, alternatively, percent values, of the new pyrazolo-pyridine compounds **10−12**. From the binding data, it can be seen that some of these compounds demonstrated moderate to high affinity for A$_1$ AR. Moreover, all of these derivatives exhibited no affinity toward both the A$_{2a}$ and the A$_3$ AR, with consequent high selectivity against A$_1$ AR.

As a general rule, compounds **10**, bearing a chlorophenylethyl side chain at the 1-position, represented the most active compounds within the newly synthesized molecules. In fact, **10k** showed the lowest affinity value against A$_1$ AR (50 nM), while compounds **10a**,**b**,**e**,**g**,**j** were characterized by affinity data ranging from 98 to 152 nM.

The length of the side chain at the C4 was of great importance for A$_1$ affinity. Reduction of the phenylethyl moiety of **10k** to a benzyl or phenyl group of **10j**,**i**, respectively, caused a relevant decrease in affinity for A$_1$ AR, probably due to the reduction of hydrophobic contacts with the receptor (see below). On the contrary, a shorter alkyl chain (*n*-propyl or cyclopropyl of compounds **10a**,**b**, respectively) was associated with higher

Table 1. Physicochemical Data and Affinity at ARs of Compounds **10**−**12**

no.	R_2	formula	mp (°C)	yield (%)	K_i (nM)[a] or % inhibition A_1[b]	A_{2a}[c]	A_3[d] (%)
10a	NHC$_3$H$_7$	C$_{20}$H$_{23}$N$_4$O$_2$Cl	82−83	90	100 ± 8.4	11%	23
10b	NHcyclopropyl	C$_{20}$H$_{21}$N$_4$O$_2$Cl	102−103	93	112 ± 9.6	10%	
10c	NHC$_4$H$_9$	C$_{21}$H$_{25}$N$_4$O$_2$Cl	81−82	70	4100 ± 23	3%	
10d	NHC(CH$_3$)$_3$	C$_{21}$H$_{25}$N$_4$O$_2$Cl	149−150	60	4800 ± 32	19%	
10e	NH(CH$_2$)$_2$OC$_2$H$_5$	C$_{21}$H$_{25}$N$_4$O$_3$Cl	108−109	80	151 ± 10	2%	
10f	NHcyclohexyl	C$_{23}$H$_{27}$N$_4$O$_2$Cl	104−105	75	1490 ± 107	0%	
10g	1-pyrrolidinyl	C$_{21}$H$_{23}$N$_4$O$_2$Cl	164−165	75	98.2 ± 7.3	17%	0
10h	4-morpholinyl	C$_{21}$H$_{23}$N$_4$O$_3$Cl	87−88	70	470 ± 29	0%	
10i	NHC$_6$H$_5$	C$_{23}$H$_{21}$N$_4$O$_2$Cl	137−138	88	348 ± 21	11%	
10j	NHCH$_2$C$_6$H$_5$	C$_{24}$H$_{23}$N$_4$O$_2$Cl	143−144	75	139 ± 10	0%	
10k	NHCH$_2$CH$_2$C$_6$H$_5$	C$_{25}$H$_{25}$N$_4$O$_2$Cl	121−122	85	50 ± 3.7	4%	34
10l	1-piperidinyl	C$_{22}$H$_{26}$N$_4$O$_2$Cl$_2$	135−136[e]	75	41%	23%	
10m	1-hexahydroazepinyl	C$_{23}$H$_{27}$N$_4$O$_2$Cl	170−171	70	35%	22%	
10n	1-(4-methylpiperazinyl)	C$_{22}$H$_{26}$N$_5$O$_2$Cl	142−143	80	22%	2140 ± 112	
11a	NHcyclopropyl	C$_{21}$H$_{24}$N$_4$O$_3$Cl$_2$	184−185[e]	86	1047 ± 97	34%	
11b	NHC$_4$H$_9$	C$_{22}$H$_{27}$N$_4$O$_3$Cl	75−76	73	1219 ± 104	23%	
11c	NH(CH$_2$)$_2$OC$_2$H$_5$	C$_{22}$H$_{28}$N$_4$O$_4$Cl$_2$	145−146[e]	50	2690 ± 192	15%	
11d	NHcyclohexyl	C$_{24}$H$_{30}$N$_4$O$_3$Cl$_2$	75−76[e]	83	3710 ± 240	1%	
11e	1-pyrrolidinyl	C$_{22}$H$_{26}$N$_4$O$_3$Cl$_2$	179−180[e]	65	33%	15%	
11f	4-morpholinyl	C$_{22}$H$_{26}$N$_4$O$_4$Cl$_2$	180−181[e]	63	40%	0%	
11g	NHCH$_2$C$_6$H$_5$	C$_{25}$H$_{25}$N$_4$O$_3$Cl	129−130	70	36%	12%	
11h	NHCH$_2$CH$_2$C$_6$H$_5$	C$_{26}$H$_{27}$N$_4$O$_3$Cl	105−106	75	456 ± 37	5%	
12a	NHC$_3$H$_7$	C$_{20}$H$_{22}$N$_4$O$_2$	147−148	82	40%	0%	
12b	NHcyclopropyl	C$_{20}$H$_{20}$N$_4$O$_2$	137−138	75	67%	0%	
12c	NHC$_4$H$_9$	C$_{21}$H$_{24}$N$_4$O$_2$	130−131	83	60%	0%	
12d	NH(CH$_2$)$_2$OC$_2$H$_5$	C$_{21}$H$_{24}$N$_4$O$_3$	139−140	98	51%	0%	
12e	NHcyclohexyl	C$_{23}$H$_{26}$N$_4$O$_2$	143−144	80	21%	0%	
12f	1-pyrrolidinyl	C$_{21}$H$_{22}$N$_4$O$_2$	151−152	90	39%	0%	
12g	4-morpholinyl	C$_{21}$H$_{22}$N$_4$O$_3$	123−124	90	40%	0%	
12h	NHCH$_2$C$_6$H$_5$	C$_{24}$H$_{22}$N$_4$O$_2$	172−173	94	39%	2%	
12i	NHCH$_2$CH$_2$C$_6$H$_5$	C$_{25}$H$_{24}$N$_4$O$_2$	156−157	95	58%	2%	

[a] The K_i values are means ± SEM of three separate assays, each performed in triplicate. [b] Displacement of specific [^{3}H]CHA binding in bovine cortical membranes or percentage of inhibition of specific binding at 10 μM concentration. [c] Displacement of specific [^{3}H]CGS$_{21680}$ binding in bovine striatal membranes or percentage of inhibition of specific binding at 10 μM concentration. [d] Displacement of specific [^{125}I]AB-MECA binding in bovine cortical membranes or percentage of inhibition of specific binding at 10 μM concentration. Only compounds **10a,g,k** were tested. [e] As hydrochloride.

Table 2. Experimental and Calculated Binding Affinity of Compounds **13**−**29** (Taken from the Literature), and **10a,e,i,k** and **11h** Belonging to the New Class of A_1AR Antagonists

compd	ref	K_i (nM)	ΔG_{exp} (kcal/mol)[a]	ΔG_{pred} (kcal/mol)	$\Delta\Delta G$ (kcal/mol)
13	13	0.19	−13.030	−12.884	0.146
14[b]	33	0.46	−12.510	−11.033	1.477
15[b]	15	2.6	−11.500	−10.694	0.806
16	34	7.3	−10.900	−10.557	0.343
17[b]	35	7.9	−10.860	−10.527	0.333
18[b]	36	10	−10.720	−10.444	−0.276
19	37	13	−10.570	−9.668	0.902
20	38	176	−9.050	−8.118	0.932
21	39	540	−8.400	−9.034	−0.634
22	40	29.5	−10.090	−10.045	0.045
23	41	0.49	−12.480	−12.913	−0.433
24	66	1.3	−11.910	−11.628	0.282
25	66	15	−10.480	−10.845	−0.365
26	19	4300	−7.190	−8.408	−1.217
27[b]	15	101	−9.374	−11.356	−1.982
28[b]	68	600	−8.337	−9.383	−1.046
29[b]	41	6.6	−10.961	−9.379	1.582
10a[b]	21	100	−9.380	−8.138	1.242
10e[b]	21	151	−9.140	−7.595	1.545
10i[b]	21	348	−8.650	−8.720	−0.070
10k[b]	21	50	−9.780	−10.045	−0.262
11h[b]		456	−8.500	−8.504	−0.007

[a] Free energies of binding derived from the K_i values according to the Gibbs−Helmholtz equation. [b] Test set ligands used for the prediction of ΔG_{pred} values.

affinity with respect to longer or bulky substituents such as the butyl or *tert*-butyl moieties of compounds **10c,d**, respectively.

Introduction of a long alkoxyalkyl chain at C4 partially restored the affinity for A_1 AR, being 151 nM the value measured for affinity of compound **10e**. Finally, variation on the nature of the amine (from secondary to tertiary) at the C4 position significantly influenced the affinity. The general trend showed a marked drop in affinity with tertiary amines, with the only exception of compound **10g** that showed appreciable affinity for A_1 AR.

When the 2-chloro-2-phenylethyl side chain at the N1 position was changed to the 2-chloro-3-phenoxypropyl moiety or to the styryl group, a dramatic decrease in affinity was observed. In fact, both compounds **11** and **12** were all characterized by very low affinity data.

These findings led to the suggestion that the extension of the alkyl chain at the C4, combined with the substituent at the N1 position, had some relevant effects on the binding of compounds **10**−**12** to the A_1 AR. When a 2-chloro-2-phenylethyl side chain was linked to the N1 position of the pyrazole ring, a gradual increase in affinity was observed by lengthening the side chain at C4 from a phenyl to a phenylethyl moiety. On the contrary, the highest affinity for the 4-alkylamino derivatives was found when the chain was characterized by three carbon atoms (*n*-propyl or cyclopropyl).

Analogous considerations cannot be made for compounds bearing a 2-chloro-3-phenoxypropyl moiety at N1. In fact, as a general rule, compounds **11** were less active than the corresponding molecules belonging to **10**. As an example, while affinity of **11h** was about 3-fold

Table 3. Intrinsic Activity of **10g**,**k** toward A_1 ARs Expressed as GTP Shift

compd	K_i (nM)[a]		GTP shift
	−GTP	+GTP	
R-PIA	4.2 ± 0.3	19.9 ± 1.4	4.7
10g	103 ± 10.4	90 ± 6.3	0.96
10k	69.7 ± 4.9	56 ± 3.6	0.8

[a] Displacement of [^{3}H]DPCPX from bovine cortical membranes in the absence (−GTP) and in the presence (+GTP) of 1 mM GTP. Values are taken from three separate experiments and expressed as means $\pm$ SEM.

Figure 2. Concentration-dependent reversal of CHA adenylyl cyclase activity inhibition by **10g** (■) and **10k** (▲) derivatives. The enzyme activity was assayed at the concentrations of the antagonists indicated in the presence of 100 nM CHA and 0.1 mM forskolin as described in biologic methods. Each data point is expressed as a percentage of adenylyl cyclase activity and represents the mean $\pm$ SEM of at least three independent experiments.

lower than the corresponding **10j**, affinity of **11a**,**c** was about 1 order of magnitude lower than **10b**,**e**, respectively.

This last evidence supported the hypothesis that the side chain at the N1 position was also a crucial key in determining the affinity values of these compounds toward A_1 AR, in agreement with results obtained from the pseudoreceptor modeling (see below). In fact, the surrogate of the A_1 AR generated by means of PrGen[25] software showed that a phenylethyl side chain at N1 possessed the optimal structural requirements (in terms of extension and bulkiness) to have profitable hydrophobic interactions with Ile6(89), Ile14(252), and His23 of the putative receptor.[26]

Results and Discussion

A computational study that combines a ligand-based drug design (pharmacophore development) method and a pseudoreceptor generation approach aimed at rationalizing the relationships between structures and affinity data of A_1 AR antagonists is presented. In particular, the combined computational approach can be summarized as follows: (i) generation of a pharmacophore model to be intended as identification and superposition of the structural features shared by the molecules and potentially important for biological activity; (ii) building of a pseudoreceptor model (based on the above alignment and on site-directed mutagenesis experiments) and its validation by prediction of the activity of the test set molecules, aligned to the pharmacophore model.

Molecular Alignment and Pharmacophore Model Generation. Several pharmacophore models for the A_1 AR ligands have already been presented in the literature,[27−35] all based on the assumption that A_1 agonists and antagonists share a common binding site on the biomolecule.[32] Among them, the most accredited is the N^6-C8 model,[30] which is derived from the greatest overall steric and hydrophobic overlap of xanthine antagonists with respect to adenosine, the natural substrate of the A_1 receptor.

Eleven structurally diverse A1 selective adenosine antagonists **13−23**[13,15,35−43] were taken from the literature (Figure 3), and the DISCO (DIStance COmparison)[44] strategy was employed to derive a meaningful pharmacophoric model for these compounds.

In the first DISCO runs, among all of the solutions proposed by the program, both the standard, the flipped, and the N^6-C8 models were found. By increasing the minimum input number of common pharmacophoric points, among all of the different hypotheses found, a seven point model with three hydrophobic centers (HY), one hydrogen bond acceptor atom (AA), one acceptor site
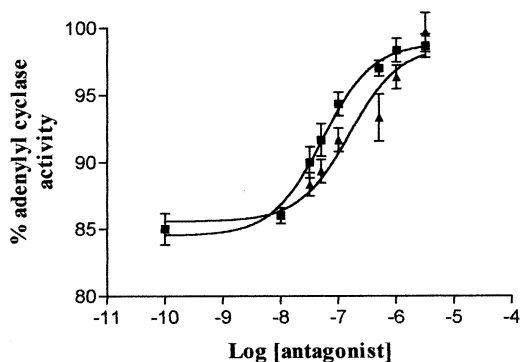
(AS), and two donor sites (DS) (tolerance 2.0 Å) was derived. Figure 4 shows the seven feature pharmacophore model with compounds **13−23** superimposed on it. As an example, compound **13**, chosen by the program as the reference molecule, is characterized by a complete mapping onto the pharmacophore model. In fact, while HY2 is matched by both the five-membered heterocyclic ring and the alkyl substituent at the 3-position, the HY3 feature is mapped by both the six-membered heterocyclic ring and the alkyl chain at the 1-position. On the other hand, HY1 is fulfilled by the adamantyl moiety at the 8-position. Moreover, the nitrogen atom at the 9-position corresponds to the AA feature of the model, with DS1 representing its counterpart on the putative receptor. Finally, the NH group at the 7-position and the carbonyl group at the 6-position are the molecular counterparts of the corresponding AS and DS2 features of the putative receptor.

The validity of the new pharmacophore was tested by means of molecular field analysis. Accordingly, for each conformer of compounds **13−23** selected by DISCO in deriving the seven point model, the corresponding electrostatic map was generated from the atomic partial charges calculated with MOPAC[45] (AM1) and compared each other with the Isopotential Contour option in Sybyl.[46] As a result, a good superimposition in isopotential contours for the selected compounds was found. Moreover, the HINT program[47] was applied to localize and display common hydrophobic areas for compounds **13−23**. The superimposition of HINT maps of the most selective compounds highlighted three hydrophobic portions of the molecules able to fit three pockets (labeled as P1, P2, and P3 in Figure 5) on the putative receptor. In detail, P1 could represent the hydrophobic region of the receptor contacted by HY1 (i.e., the alkyl substituent at the 8-position of **13**). Similarly, P2 defines a hydrophobic cavity where alkyl or aryl substituents lie and where the N3 substituent of xanthinic antagonists, such as **13**, is located. Finally, P3 is the region of the receptor able to accept various substituents, in particular the N1 substituent of compound **13**.

All of these findings showed a good agreement between the properties of the pharmacophore model generated by DISCO and the results obtained by means
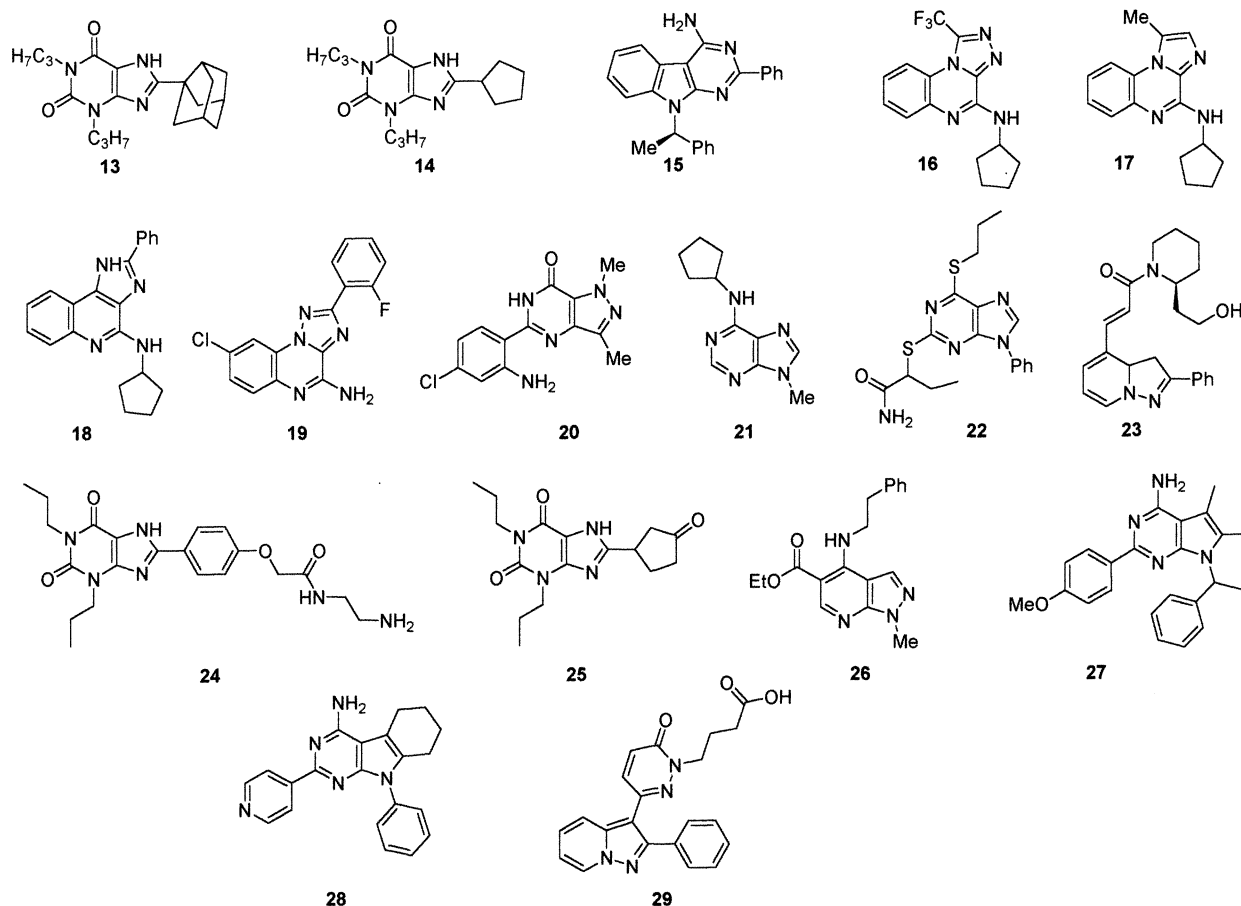
Figure 3. Compounds **13**−**29** collected from the literature and used for pharmacophore generation and pseudoreceptor modeling.
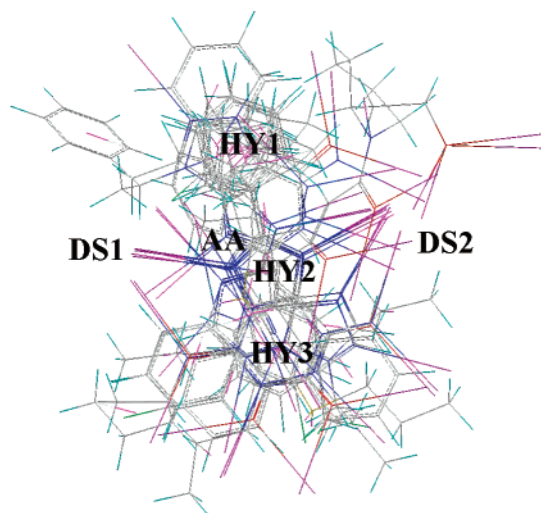

Figure 4. DISCO superposition of compounds **13**−**23**. Pharmacophore features are labeled with AA (hydrogen bond acceptor atom), HY (hydrophobic center), DS (donor site), and AS (acceptor site).
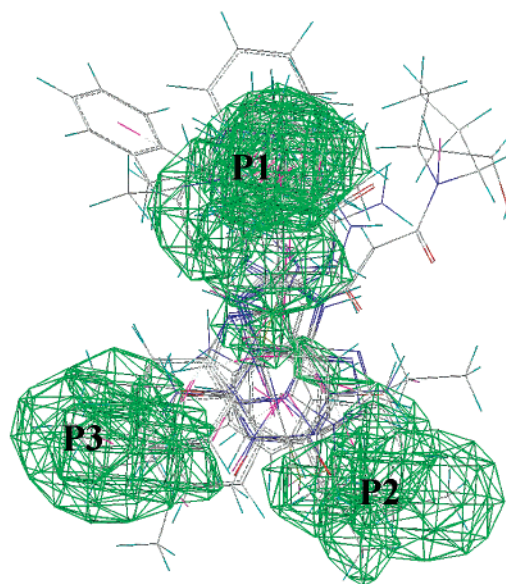

Figure 5. HINT maps for compounds **13**−**23**. Green volumes represent the hydrophobic regions occupied by the ligand corresponding to the P1, P2, and P3 pockets on the putative receptor.

of HINT calculations. In fact, while P2 and P3 pockets partially fit the HY1 and HY3 features of the pharmacophore model, HY1 and P1 are perfectly superposed.

In summary, DISCO and HINT calculations improved the previous N^6-C8 model with a novel seven point pharmacophoric map whose properties can be summarized as follows: (i) a hydrogen bond acceptor atom (AA) corresponding to a nitrogen or oxygen atom, able to interact with a donor site (DS1), which represents the counterpart on the receptor; (ii) two hydrophobic centers (HY2 and HY3) in the bicyclic planar nucleus filling the corresponding receptor pockets P2 and P3 and a third hydrophobic center (HY1) on the side chain matching the P1 receptor pocket; (iii) one acceptor site (AS) and two donor sites (DS1 and DS2), which define the putative active site on the A_1 receptor.

Pseudoreceptor Generation. The pharmacophore model (corresponding to the alignment of the ligands deduced by DISCO calculations) was used to perform the second computational step of our work. Particularly, by application of the pseudoreceptor modeling software PrGen, an atomistic binding site model for A_1 AR was built taking into account the structure and biological activity of known ligand molecules.

For the generation of the pseudoreceptor model, with the aim of covering a range of about 4−5 orders of magnitude in affinity, six additional antagonists (**24**−**29**)[15,19,43,48,49] taken from the literature were considered. They all express antagonist activity toward A_1 AR and were collected under the assumption that all of these substances were acting through the same binding site.

Biological data of the whole set of compounds **13**−**29**, expressed as K_i, were in the range between 0.19 (compound **13**) and 4300 nM (compound **26**). According to the Gibbs−Helmholtz equation, K_i values were converted into free energies of binding, hereafter reported as ΔG_{exp}. Ten molecules of the whole set (namely, compounds **13**, **16**, and **19**−**26** reported in Table 2) have been automatically chosen by PrGen to build the training set.

Next, to choose appropriate residues for pseudoreceptor construction, information derived from site-directed mutagenesis experiments[3c,6,50] and from the primary amino acid sequence of the rat A_1 AR,[51] were used. Moreover, the receptor-mediated ligand alignment technique[52,53] was applied to generate the primordial model (see the Experimental Section for further details). In the next step, the remaining seven ligands of the training set were docked into the receptor cavity thus generating the final pseudoreceptor−inhibitors assembly.

To achieve the optimum positions of the manually placed residues, a receptor equilibration was subsequently performed allowing for translation, rotation, and torsional variations of receptor residues, whereas the ligands were kept fixed in their original arrangements (correlation-coupling protocol). Finally, the pharmacophore was allowed to relax within the binding pocket. Repeating these two steps several times (the computational protocol called ligand equilibration) yielded a pseudoreceptor model with an r value of 0.93 and rmsd between experimental and predicted free energies of ligand binding of 0.641 kcal/mol, corresponding to an uncertainty factor of 3.0 in the inhibitory constants.

Comparison between the Pseudoreceptor and the Pharmacophore Model. Figure 6 and Scheme 2 show the complex between the final pseudoreceptor model and the compound **13**, taken as representative of all of the A_1 AR inhibitors considered in this study. The pseudoreceptor is mainly characterized by a large hydrophobic pocket defined by Ile14(252), Leu15(253), Ile18(272), Ala19(273), and Ile20 (details on residue numbering are given in ref 26), and two distinct hydrogen-bonding sites involving Thr1(91) and His12-(251), respectively.

The hydrophobic cavity is able to accommodate bulky cycloalkyl substituents, such as the noradamantyl moiety of **13**, mainly interacting with the alkyl side chain of Ile20. Moreover, a polar substitution at the 8-position of the xanthine nucleus is also tolerated. As an example,
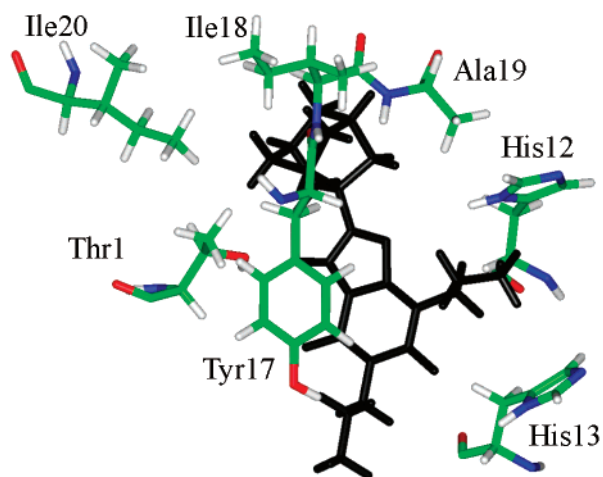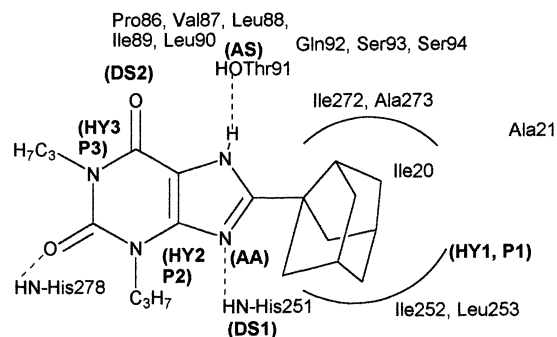

Figure 6. Complex between the A_1 adenosine pseudoreceptor (green) and the compound **13** (black), the most active inhibitor considered in this study. For the sake of clarity, only few amino acids of the model have been displayed.

Scheme 2. Schematic representation of residues constituting the pseudoreceptor model and their major interactions with compound **13**[a]

[a] Amino acid labels are from the primary sequence of rat A_1AR (see ref 26 for further detail). In parentheses, pharmacophore features identified by DISCO and HINT calculations.

the terminal amino group of the long hydrophilic side chain of **24** is engaged in a hydrogen-bonding contact with the carbonyl moiety of Ala21. Ile14(252) and Leu15(253) of the hydrophobic pocket are located in a region of the space in front of the five-membered ring of the xanthine nucleus, thus corresponding to the receptor counterpart of the HY1 hydrophobic feature identified by DISCO. Ile18(272) and Ala19(273), constituting a portion of the hydrophobic pocket containing the C8 substituent, are located at the opposite site of the five-membered ring, with respect to Ile14(252) and Leu15(253).

The nitrogen atom at the 9-position interacts by a hydrogen bond with the NH group of the imidazole ring of His12(251), the NH−N9 distance being 3.01 Å. As a consequence, the xanthine N9 and the His12(251) NH group could be identified as the AA and DS1 features of the DISCO pharmacophore, respectively. In a similar way, the xanthine NH group at the 7-position is involved in a hydrogen-bonding interaction with the hydroxy oxygen of Thr1(91) (NH−O distance of 1.76 Å) corresponding to the AS pharmacophore feature.

Finally, while the aromatic portion of Tyr17(271) is located at the proper distance of about 4.6 Å to have profitable interactions with the six-membered ring of xanthines (based on a T-tilted orientation of the two

cyclic moieties), Gln2(92) and Leu7(88) approach the region accommodating the N1 and C6 positions of **13**, thus corresponding to the HY3 feature.

In summary, to depict the major interaction keys between pseudoreceptors and inhibitors, we can additionally report that the hydroxy oxygen of Thr1(91) acts as a hydrogen-bonding acceptor for the hydrogen atom bound to N7 in the xanthine derivatives (such as **13**, **24**, and **25**), as well as for the hydrogen atom bound to N^6 of nonxanthine derivatives **16** and **21** and at the 1-position of **20**. This result is in accordance with site-directed mutagenesis data suggesting an interaction between Thr1(91) and the N^6 substituents of adenine moiety in antagonist compounds.[3c] On the other hand, the imidazole NH hydrogen of His12(251) (reported as an important amino acid for interactions with A1 antagonists)[50b] is engaged in a hydrogen bond interaction with the N9 nitrogen atom of **13** and **19**. Moreover, the terminal amino group on the long C8 side chain of compounds **24** is involved in an additional hydrogen bond with the carbonyl oxygen of Ala 21. Finally, the hydrophobic cavity accommodates the bulky substituent at the 8-position of xanthine antagonists and at the N^6-position of adenosine analogues, according to the N^6-C8 pharmacophore model.

Validation of the Pseudoreceptor Model. With the purpose of testing the predictive power of the model, 12 A1 antagonists defining the test set (Table 2) were docked into the receptor model following the DISCO-derived alignment and subjected to a free ligand relaxation with the same settings used for the training set. This procedure yielded a rmsd between experimental and predicted free energies of ligand binding of 1.1 kcal/mol, corresponding to an uncertainty factor of 6.6 in the inhibitory constants.

Although the theoretically derived pseudoreceptor model is unlikely to fully describe the real binding site of A_1 AR, it was able to explain the properties of the new synthesized antagonists. In fact, the most active ligand of the series, **10k**, bearing a 2-chloro-2-phenylethyl side chain at the N1 nitrogen atom together with a phenylethylamino substituent at the C4 carbon atom, is predicted by the model to have a ΔG of -10.045 vs an experimental value of -9.780 kcal/mol. Compound **10k** interacts with the pseudoreceptor model in such a way as its C4 side chain contacts a hydrophobic region mainly defined by Leu15(253), Ala19(273), and Ile20. On the other hand, while the side chain at the N1 position is located inside a second pocket surrounded by Gln2(92), Ser13(281), and Glu22, the ethyl ester chain at the 5-position is embedded between His10(278) and His12(251). It is also important to point out that the pyridine ring of the bicyclic nucleus is involved in a $\pi-\pi$ interaction with the aromatic side chain of Tyr17-(271).

The shortening of the C4 phenylethylamino to a benzylamino or phenylamino substituent (compound **10j,i**, respectively) lead to reduced hydrophobic contacts between the ligand and the pseudoreceptor (particularly, Ile20). Accordingly, the estimated binding free energy of **10i** was -8.720 kcal/mol vs an actual value of -8.650 kcal/mol.

On the other hand, when the C4 substituent is an alkylamino (**10a**) or alkoxyalkylamino (**10e**) group, the affinities of such compounds were predicted to be -8.138 and -7.595 kcal/mol vs actual values of -9.380 and -9.140 kcal/mol, respectively. Also in this case, we may interpret this decrease in affinity taking into account that both the alkyl and the alkoxyalkyl chains lack some of the profitable hydrophobic contacts with Leu15(253), Ala19(273), and Ile20 found for compound **10k**.

Moreover, the molecular portion corresponding to the C5–C6 sequence of the heterocycle is accommodated within a pseudoreceptor cavity mainly defined by His12-(251), His13(278), Tyr17(271), and Ala19(273) (containing the HY2 pharmacophore feature described below in the text), quite unexplored by our derivatives. In fact, while the carbethoxy substituent of compounds **10–12** corresponded to the propyl chain at the 4-position of **13**, the condensed phenyl ring of active compounds such as **16** and **17** is located in front of the unsubstituted C6 of the pyrazolo-pyridine nucleus. These findings led to the suggestion that variations on the stereoelectronic properties of the carbethoxy substituent are required, as well as insertion of lipophilic moieties into the C6 position of the pyrazole-pyridine ring.

Finally, variation on the length of the N1 substituent also affects the affinities of these derivatives. Particularly, the lengthening (from a 2-chloro-2-phenylethyl to a 2-chloro-3-phenoxypropyl moiety) of the side chain at the N1 position of **11h** lead to a decreased affinity (-8.505 estimated vs -8.497 kcal/mol experimental value) mainly due to unfavorable contacts between the phenoxy moiety and the His23 residue.

Comparison between the Proposed Pharmacophore and Pseudoreceptor Models and Previously Published Models for A_1 AR. A recent paper[23] described both a pharmacophore model for A_1 AR and the three-dimensional theoretical models of the complexes between compounds taken from the literature (i.e., compound **18**) and a putative A_1 AR, as determined by homology modeling and molecular dynamics calculations. Having no structural information (i.e., distances between the key structural elements of these complexes) in our hands, we could make only a qualitative comparison between these structures and the pharmacophore model proposed in this paper.

In particular, a perfect agreement has been found between the pharmacophore model proposed by Da Settimo and results derived from both our DISCO and our HINT studies. In fact, the hydrogen bond acceptor–donor features identified by DISCO and the three hydrophobic pockets found with HINT were all described in the cited paper. On the other hand, some differences have been highlighted by comparing our pseudoreceptor and the complexes previously reported. In detail, the Asn254 side chain has been reported by Da Settimo as responsible for a hydrogen bond acceptor–donor motif involving both N^6 and N7 of compound **18**. On the contrary, the corresponding Asn16(254) of our pseudoreceptor is at the periphery of the binding site, while the N^6 atom of **18** interacts by a hydrogen bond with the hydroxy group of Thr1(91), in agreement with Rivkees and co-workers[3c] reporting the same residue as interacting with the N^6 substituents of A_1 AR ligands. Moreover, to the best of our knowledge, no experimental data have been published on the literature supporting the hypothesis that Asn254 can represent

the receptor residue interacting with the hydrogen-bonding acceptor−donor motif of A_1 antagonists. As a consequence, the pharmacophore model proposed by our research group, reproducing the well-known N^6-Thr91 interaction, could be considered as an improved model with respect to the Da Settimo hypothesis.

Moreover, the hydrophobic region corresponding to the P3 pocket described in this paper has been suggested by Da Settimo as a relatively small cavity, not in full agreement with our results. In fact, the pseudoreceptor model is able to well-accommodate within the P3 pocket the phenylethyl side chain of compound **10k**, the most active molecule in our hands. Particularly, while the phenyl ring is mainly interacting with His23, the ethyl portion of the side chain maps a region defined by His10(270), Ser13(281), and Ile14(252). These findings led to the suggestion that the size of P3 is able to accommodate extended, not too bulky, side chains.

Finally, while the Da Settimo model, based on pharmacophore generation and molecular docking protocols, allowed for the rationalization of A_1 AR antagonist SAR only at a qualitative level, our pseudoreceptor provided quantitative relationships between the structure of A_1 AR antagonists and their biological data.

Conclusions

A pharmacophore model generation protocol has been successfully applied to build a three-dimensional model of the chemical features responsible for A_1 AR antagonist activity. The seven pharmacophore features corresponded to four structural portions on the ligands and three points of the receptor, mapping the most important interaction between the A_1 receptor and its antagonists.

The pharmacophore model, combined with the findings derived from experimental data (site-directed mutagenesis and primary amino acid sequence of rat A_1 AR), was used to build a pseudoreceptor, to be intended as the putative binding site model for the structurally uncharacterized A_1 AR. Such a three-dimensional receptor surrogate has been subsequently validated using an external set of compounds (test set), leading to high correlation and predictive power as well as a good agreement with the pharmacophore model.

The newly synthesized compounds showed an interesting antagonistic profile and selectivity toward A_1 ARs, with respect to molecules belonging to the same class of pyrazolo-pyridine derivatives reported in the literature. The pseudoreceptor appeared to be an improved model with respect to both the N^6-C8 hypothesis and a three-dimensional model of A_1 AR recently described in the literature. It also furnished some suggestions on variations that should be made on the structure of the pyrazolo-pyridine compounds to better fit the pseudoreceptor model. In particular, C5 and C6 were identified as the positions to be further investigated. Accordingly, enlargement of the pyrazolo-pyridine class is ongoing by synthesis of some new derivatives that will be published in due time with their biological data.

Experimental Section

Chemistry. Starting materials were purchased from Aldrich-Italia (Milan). Melting points were determined with a Büchi 530 apparatus and are uncorrected. IR spectra were measured in KBr with a Perkin-Elmer 398 spectrophotometer. ^{1}H NMR spectra were recorded in $(CD_3)_2SO$ solution on a Varian Gemini 200 (200 MHz) instrument. Chemical shifts are reported as δ (ppm) relative to tetramethylsilane (TMS) as internal standard, J in Hz. ^{1}H patterns are described using the following abbreviations: s = singlet, d = doublet, t = triplet, q = quartet, sx = sextect, m = multiplet, br = broad. All compounds were tested for purity by thin-layer chromatography (TLC) (Merk, Silica gel 60 F_{254}, $CHCl_3$ as eluant). Analyses for C, H, N were within ±0.3% of the theoretical value.

5-Amino-1-(2-hydroxy-2-phenylethyl)-1H-pyrazole-4-carboxylic Acid Ethyl Ester (5a). The starting hydrazine **3a** (3.04 g, 20.0 mmol) was added to a solution of ethyl-ethoxymethylene cyanoacetate **4** (3.38 g, 20.0 mmol) in anhydrous toluene (20 mL), and the mixture was heated at 80 °C for 8 h. The solution was then concentrated by rotatory evaporation to half of the volume and allowed to cool to room temperature.

The separated yellow pale solid was filtered and recrystallized from toluene to afford **5a** (4.40 g, 80%) as a white solid; mp 136−137 °C. ^{1}H NMR (CDCl$_3$): δ 1.33 (t, J = 7.0, 3H, CH$_3$), 3.53 (m, 1H, OH, disappears with D$_2$O), 3.92−4.20 (m, 2H, CH$_2$N), 4.25 (q, J = 7.0, 2H, CH$_2$O), 5.02−5.13 (m, 1H, CHOH), 5.30 (br s, 2H, NH$_2$, disappears with D$_2$O), 7.23−7.42 (m, 5H Ar), 7.58 (s, 1H, H-3). IR (CHCl$_3$) cm^{-1}: 3470, 3330 (NH$_2$), 3300−3000 (OH), 1685 (CO). Anal. (C$_{14}$H$_{17}$N$_3$O$_3$) C, H, N.

5-Amino-1-(2-hydroxy-3-phenoxy-propyl)-1H-pyrazole-4-carboxylic Acid Ethyl Ester (5b). The compound was prepared according to the synthetic sequence described for compound **5a** starting from **3b** to give **5b** as a white solid (4.88 g, 80%); mp 94−95 °C. ^{1}H NMR (CDCl$_3$): δ 1.33 (t, J = 7.1, 3H, CH$_3$), 2.5−3.5 (very br s, 1H, OH, disappears with D$_2$O), 3.82−4.06 and 4.15−4.33 (2m, 4H, CH$_2$N + CH$_2$OAr), 4.26 (q, J = 7.1, 2H, CH$_2$OCO), 4.36−4.49 (m, 1H, CHO), 5.1−5.7 (very br s, 2H, NH$_2$, disappears with D$_2$O), 6.85−7.05 and 7.22−7.38 (2m, 5H Ar), 7.63 (s, 1H, H-3). IR (CHCl$_3$) cm^{-1}: 3600−3450 and 3350 (OH + NH$_2$), 1680 (CO). Anal. (C$_{15}$H$_{19}$N$_3$O$_4$) C, H, N.

5-Amino-1-(2-hydroxy-2-phenylethyl)-1H-pyrazole-4-carboxylic Acid (6a). To a solution of **5a** (2.7 g, 10 mmol) in ethanol 96% (15 mL), a solution 3.5 M of NaOH (10 mL) was added. The reaction mixture was refluxed for 4 h, and then, the ethanol was evaporated under reduced pressure. The mixture was acidified with HCl 6 N; the precipitated white solid was collected by filtration and washed with water. The crude product was then recrystallized from absolute ethanol to give **6a** as a white solid (2.34 g, 95%); mp 180−182 °C (dec). ^{1}H NMR ((CD$_3$)$_2$SO): δ 3.92−4.25 (m, 2H, CH$_2$N), 4.91−5.03 (m, 1H, CHOH), 5.68−5.76 (m, 1H, OH, disappears with D$_2$O), 6.03−6.13 (br s, 2H, NH$_2$, disappears with D$_2$O), 7.23−7.44 (m, 5H Ar), 7.45 (s, 1H, H-3), 11.50−12.00 (br s, 1H, COOH, disappears with D$_2$O). IR (KBr) cm^{-1}: 3385, 3280 (NH$_2$), 3250−2800 (COOH + OH), 1650 (CO). Anal. (C$_{13}$H$_{13}$N$_3$O$_3$) C, H, N.

5-Amino-1-(2-hydroxy-3-phenoxy-propyl)-1H-pyrazole-4-carboxylic Acid (6b). The compound was prepared according to the synthetic sequence described for compound **6a** starting from **5b**, to give **6b** (2.49 g, 90%) as a white solid; mp 152−153 °C (dec). ^{1}H NMR ((CD$_3$)$_2$SO): δ 3.82−4.35 (m, 5H, 2CH$_2$ + CH), 5.41−5.62 (m, 1H, OH, disappears with D$_2$O), 5.95−6.25 (br s, 2H, NH$_2$, disappears with D$_2$O), 6.80−7.10 and 7.15−7.32 (2m, 5H Ar), 7.50 (s, 1H, H-3), 11.50−12.05 (br s, 1H, COOH, disappears with D$_2$O). IR (KBr) cm^{-1}: 3435, 3310 (NH$_2$), 3200−2500 (OH), 1670 (CO). Anal. (C$_{13}$H$_{15}$N$_3$O$_4$) C, H, N.

2-(5-Amino-pyrazol-1-yl)-1-phenyl Ethanol (7a). Compound **6a** (2.47 g, 10 mmol) was heated to 185 °C. When the development of CO$_2$ had finished, the residue was cooled to room temperature, dissolved in HCl 6 N, and neutralized with solid NaHCO$_3$. A light brown solid precipitated, which was collected by filtration. The crude product was then recrystallized from CHCl$_3$ to give **7a** (1.99 g, 98%) as a light yellow solid; mp 130−132 °C. ^{1}H NMR (CDCl$_3$): δ 1.70−3.20 (br s, 3H, NH$_2$ + OH, disappears with D$_2$O), 4.03−4.31 (m, 2H, CH$_2$),

5.09–5.19 (dd, 1H, CHOH), 5.54 (d, 1H, H-4), 7.20–7.50 (m, 6H, 5H Ar + H-3). IR (CHCl₃) cm⁻¹: 3500–3000 (OH + NH₂). Anal. (C₁₁H₁₃N₃O) C, H, N.

1-(5-Amino-pyrazol-1-yl)-3-phenoxy-2-propan-2-ol (7b). The compound was prepared according to the synthetic sequence described for compound **7a**, starting from **6b** to give **7b** (1.98 g, 85%) as a light yellow solid; mp 112–113 °C. ¹H NMR (CDCl₃): δ 1.70 (br s, 1H, OH, disappears with D₂O), 3.72–3.99 (m, 4H, CH₂N + NH₂, 2H disappear with D₂O), 4.13–4.29 (m, 2H, CH₂O), 4.30–4.48 (m, 1H, CHOH), 5.50–5.53 (m, 1H, H-4), 6.38–7.06 and 7.21–7.39 (2m, 6H, 5H Ar + H-3). IR (CHCl₃) cm⁻¹: 3500–3100 (OH + NH₂). Anal. (C₁₂H₁₅N₃O₂) C, H, N.

2-{[2-(2-Hydroxy-2-phenyl-ethyl)-2H-pyrazol-3-ylamino]methylene}malonic Acid Diethyl Ester (8a). Diethyl ethoxymethylenemalonate (2.27 g, 10 mmol) was added to **7a**, and the mixture was heated to 120 °C for 2 h and then cooled to room temperature. After diethyl ether (20 mL) was added, a white solid precipitated. The crude product was filtered off and then recrystallized from absolute ethanol to give **8a** (3.47 g, 93%) as a white solid; mp 128–129 °C. ¹H NMR (CDCl₃): δ 1.31 and 1.37 (2t, 6H, 2CH₃), 1.6–1.8 (br s, 1H, OH disappears with D₂O), 4.12–4.38 (m, 6H, 3CH₂), 5.07–5.18 (dd, 1H, CHO), 6.06 (d, 1H, H-3), 7.25–7.47 (m, 6H, 5H Ar + H-4), 8.02 (d, 1H, CH=), 11.16 (d, 1H, NH, exchanges with D₂O). IR (CHCl₃) cm⁻¹: 3400–3100 (OH + NH), 1690, 1655 (CO and C=C). Anal. (C₁₉H₂₃N₃O₅) C, H, N.

2-{[2-(2-Hydroxy-3-phenoxy-propyl)-2H-pyrazol-3-ylamino]methylene}malonic Acid Diethyl Ester (8b). The compound was prepared according to the synthetic sequence described for compound **10a** starting from **7b**, to give **8b** (2.82 g, 70%) as a light yellow solid; mp 72–73 °C. ¹H NMR (CDCl₃): δ 1.30 and 1.36 (2t, 6H, 2CH₃), 2.60–3.00 (very br s, 1H, OH, disappears with D₂O), 3.71–4.02 and 4.17–4.40 (2m, 8H, 4CH₂), 4.42–4.52 (m, 1H, CH), 6.08 (d, 1H, H-4), 6.85–7.03 and 7.21–7.32 (2m, 5H Ar), 7.45 (d, 1H, H-3), 8.08 (d, 1H, CH=), 11.16 (d, 1H, NH, exchanges with D₂O). IR (CHCl₃) cm⁻¹: 3400–3100 (OH + NH), 1685, 1655 (CO and C=C). Anal. (C₂₀H₂₅N₃O₆) C, H, N.

4-Chloro-1-(2-chloro-2-phenyl-ethyl)-1H-pyrazolo[3,4-b]pyridine-5-carboxylic Acid Ethyl Ester (9a). POCl₃ (14 g, 91 mmol) was added to **8a** (3.73 g, 10 mmol), and the mixture was refluxed for 12 h and then cooled to room temperature. The excess of POCl₃ was removed by distillation under reduced pressure. H₂O (20 mL) was then carefully added to the residue, and the suspension was extracted with CHCl₃ (3 × 20 mL). The organic solution was washed with H₂O (10 mL), dried (MgSO₄), filtered, and concentrated under reduced pressure. The crude brown oil was purified by column chromatography (Florisil 100–200 Mesh) using CHCl₃ as eluant to afford the pure product **9a** (2.18 g, 60%) as a white solid; mp 72–73 °C. ¹H NMR (CDCl₃): δ 1.44 (t, J = 7.1, 3H, CH₃), 4.45 (q, J = 7.1, 2H, CH₂O), 4.85–4.95 and 5.05–5.20 (2 dd, 2H, CH₂N), 5.52–5.62 (m, 1H, CHCl), 7.25–7.51, (m, 5H Ar), 8.21 (s, 1H, H-3), 9.02 (s, 1H, H-6). IR (CHCl₃) cm⁻¹: 1710 (CO). Anal. (C₁₇H₁₅N₃O₂Cl₂) C, H, N.

4-Chloro-1-(2-chloro-3-phenoxy-propyl)-1H-pyrazolo-[3,4-b]pyridine-5-carboxylic Acid Ethyl Ester (9b). The compound was prepared according to the synthetic sequence described for compound **9a** starting from **8b**, to give **9b** (1.97 g, 50%) as a white solid; mp 70–71 °C. ¹H NMR (CDCl₃): δ 1.45 (t, J = 7.1, 3H, CH₃), 4.28 (d, 2H, CH₂N), 4.46 (q, J = 7.1, 2H, CH₂OCO), 4.76–4.92 (m, 1H, CHCl), 4.97–5.04 (d, 2H, CH₂OAr), 6.84–7.03 and 7.22–7.57 (2m, 5H Ar), 8.25 (s, 1H, H-3), 9.03 (s, 1H, H-6). IR (CHCl₃) cm⁻¹: 1720 (CO). Anal. (C₁₈H₁₇N₃O₃Cl₂) C, H, N.

Method A. Example. 4-Propylamino-1-(2-chloro-2-phenylethyl)-1H-pyrazolo[3,4-b]pyridine-5-carboxylic Acid Ethyl Ester (10a). To a solution of **9a** (10 mmol) in anhydrous toluene (20 mL), propylamine (40 mmol) was added, and the reaction mixture was stirred at room temperature for 24 h. After it was extracted with H₂O, the organic phase was dried (MgSO₄) and evaporated under reduced pressure; the oil residue crystallized by adding absolute ethanol (10 mL) to give

10a in 90% yield; mp 82–83 °C. ¹H NMR (CDCl₃): δ 1.10 (t, J = 7.4, 3H, CH₃ prop), 1.39, (t, J = 7.1, 3H, CH₃), 1.82 (sx, J = 7.4, 2H, CH₂ prop), 3.52–3.67 (m, 2H, CH₂NH), 4.33 (q, J = 7.1, 2H, CH₂O), 4.71–4.85 and 4.97–5.12 (2 dd, 2H, CH₂N), 5.53–5.68 (m, 1H, CHCl), 7.25–7.40 and 7.42–7.52 (2m, 5H Ar), 8.03 (s, 1H, H-3), 8.87 (s, 1H, H-6), 9.21 (br s, 1H, NH, exchanges with D₂O). IR (CHCl₃) cm⁻¹: 3280 (NH), 1663 (CO).

Method B. Example. 4-Propylamino-1-styryl-1H-pyrazolo[3,4-b]pyridine-5-carboxylic Acid Ethyl Ester (12a). DBU (5 g, 33.44 mmol) was added to **10a** (10 mmol), and the mixture was heated at 90 °C for 8 h. Absolute ethanol (5 mL) was added to give the crude **12a**, which was then recrystallized from absolute ethanol with a 40% yield; mp 147–148 °C. ¹H NMR (CDCl₃): δ 1.23 (t, J = 7.4, 3H, CH₃ prop), 1.41 (t, J = 7.2, 3H, CH₃), 1.85 (sx, J = 7.4, 2H, CH₂ prop), 3.56–3.70 (m, 2H, CH₂N), 4.35 (q, J = 7.2, 2H, CH₂O), 7.20–7.43 and 7.51–7.60 (2m, 6H, 5H Ar + CH=), 8.12 (d, J = 14.8, 1H, CH=), 8.14 (s, 1H, H-3), 8.88 (s, 1H, H-6), 9.29 (br s, 1H, NH, exchanges with D₂O). IR (CHCl₃) cm⁻¹: 1655 (CO).

Biological Methods. [³H]CHA, [¹²⁵I]AB-MECA, [³H]CGS 21680, and [α³²P]ATP were obtained from DuPont-NEN (Boston, MA). DPCPX was purchased from RBI (Natik, MA). Adenosine deaminase was from Sigma Chemical Co. (St. Louis, MO).

A₁ and A₂ₐ Receptor Binding. Displacement of [³H]CHA (31 Ci/mmol) from A₁ AR in bovine cortical membranes and of [³H]CGS 21680 (42.1 Ci/mmol) from A₂ₐ AR in bovine striatal membranes was performed as described.[54] Adenosine A₁ receptor affinities with [³H]DPCPX as radioligand were determined according to Pirovano et al.[55] Measurements with [³H]DPCPX were performed in the presence and in the absence of 1 mM GTP.

A₃ AR Receptor Binding. [¹²⁵I]AB-MECA binding to A₃ AR in bovine cortical membranes was performed in 50 mM Tris, 10 mM MgCl₂, and 1 mM EDTA buffer (pH 7.4) containing 0.2 mg of proteins, 2 U/mL adenosine deaminase, and 20 nM DPCPX.[23a] Incubations were carried out in duplicate for 90 min at 25 °C. Nonspecific binding was determined in the presence of 50 μM R-PIA and represented approximately 30% of the total binding. The binding reaction was terminated by filtration through a Whatman GF/C filter, washing three times with 5 mL of ice-cold buffer.

All compounds were routinely dissolved in dimethyl sulfoxide (DMSO) and diluted with assay buffer to the final concentration, where the amount of DMSO never exceeded 2%. At least six different concentrations spanning 3 orders of magnitude, adjusted appropriately for the IC₅₀ of each compound, were used. IC₅₀ values, computer-generated using a nonlinear regression formula on a computer program (Graph-Pad, San Diego, CA), were converted to K_i values, knowing the K_d values of radioligands in the different tissues and using the Cheng and Prusoff equation.[56] The dissociation constants (K_d) of [³H]CHA, [³H]CGS 21680, and [¹²⁵I]AB-MECA were 1.2, 14, and 1.02 nM, respectively.

Adenylyl Cyclase Assay. The adenylyl cyclase assay was performed as previously described.[57] The adenylyl cyclase activity was measured by monitoring the conversion of [α³²P]-ATP to [α³²P]cAMP.[58] The method involved addition of [α³²P]-ATP to membranes in the presence of forskolin to stimulate adenylyl cyclase and papaverine as a phosphodiesterase inhibitor. Briefly, enzyme activity was routinely assayed in a 100 μL reaction mixture containing 50 mM HEPES/NaOH buffer, pH 7.4, 2 mM MgCl₂, 1 mM DTT, 0.1 mg/mL creatine phosphokinase, 0.1 mg/mL bacitracin, 0.5 mg/mL creatine phosphate, 0.1 mM ATP, 0.05 mM cAMP, 15 units/mL myo-kinase, 2 units/mL adenosine deaminase, 10 M GTP, 1 μCi [α³²P]ATP, 0.2 mM papaverine, and 0.1 mM forskolin. The incubation was started by the addition of membranes (10–20 g of proteins) and carried out for 15 min at 23 °C. The reaction was terminated by placing assay tubes in an ice bath and adding 0.5 mL of a stop solution containing 120 mM Zn-(C₂H₃O₂)₂/[³H]cAMP (10 000–20 000 cpm/sample) and then 0.6 mL of 144 mM Na₂CO₃. The total radiolabeled cAMP was

isolated on columns of Dowex 50 ion-exchange resin and albumina as described.[58]

The antagonist behavior of some compounds was examined for their ability to completely reverse the inhibition of forskolin-stimulated adenylyl cyclase activity induced by the A_1 selective agonist CHA. Experiments were performed evaluating the effects of multiple antagonist concentrations (10 nM to 10 μM) on the inhibition of adenylyl cyclase activity induced by 100 nM CHA. The compounds tested were dissolved in DMSO and then diluted with 50 mM HEPES/NaOH buffer, pH 7.4, so that the final DMSO concentration never exceeded 1%. The data were analyzed as competition curves and by nonlinear regression analysis for models of one or two noninteracting sites (GraphPad).

Molecular Modeling. All calculations were performed in vacuo, on Indigo 2 and Octane R12000 Silicon Graphics workstations. A set of seventeen structurally diverse A_1 AR selective antagonists **13**−**29** (Figure 3 and Table 2) was taken from the literature. The selection was performed on the basis of two rules: (i) the greatest structural diversity, essential requirement for obtaining a meaningful model, and (ii) K_i values spanning among ~4−5 orders of magnitude, to evaluate which pharmacophoric elements were necessary to the antagonist for displaying the highest degree of selectivity. When available,[59] X-ray data were used as starting geometries; otherwise, the interactive building procedure of MacroModel[60] was applied to draw the initial geometries to be submitted to the energy minimization protocol. A conformational analysis was carried out with the AMBER* force field, using two different strategies, which depended on the number of significant rotatable bonds present in the molecule. Systematic nested rotation of each selected dihedral angle was performed for compounds with two or less rotatable bonds, employing 10 degree increments and energy-minimizing the resulting conformations. On the contrary, the conformational space of more flexible compounds was explored by random search, using the Monte Carlo option implemented in MacroModel. Starting from different randomly generated initial conformations, several parallel Monte Carlo cycles were run. For each cycle, the following parameters were used automatic setup and 1000 as the maximum number of search interactions. Both in the systematic and in the random approach, conformations with energy higher than 5 kcal/mol above the minimum energy conformer were discarded. The selection of this energy cutoff value was based on the hypothesis that for a majority of ligand−protein complexes, the bioactive conformations are within such a threshold.[61] The search was stopped when results from different runs were nearly identical.

The high number of conformations produced by each cycle was reduced by means of a cluster analysis (XCluster option). Resulting geometries of the selected low energy conformers were reoptimized with semiempirical quantum mechanics calculations, using the Hamiltonian AM1 as implemented in MOPAC package.

The DISCO approach, as implemented in Sybyl, was subsequently applied to derive an optimal superimposition of the selected structures. Among the diverse solutions provided by the program, the selection of a meaningful pharmacophore model was done choosing the one with the highest number of pharmacophoric points and the lowest tolerance value, an index of the validity of the alignment, usually ranging from 0.5 to 2.5 Å. For all of the conformers of compounds **13**−**23** selected by DISCO, molecular electrostatic potentials and hydropathic fields were calculated, using MOPAC (AM1) and HINT computational packages, respectively. The HINT hydrophobic fields were calculated with the Essential Hydrogen Treatment and via Bond Polar Proximity. Next, while the pseudoreceptor generator software PrGen was employed to build an atomistic binding site model for the A_1 AR, a method originally developed by Marengo and Todeschini[62] and adapted for pseudoreceptor modeling by Vedani and co-workers[52] was applied to select a training set from compounds **13**−**29**.

To circumvent problems associated with the mutual obscuring of functional groups within a pharmacophore hypothesis,

the technique referred to as receptor-mediated ligand alignment was used.[52,53] In particular, at the beginning, only three compounds of the whole training set (**13**, ΔG_{exp} = −13.030 kcal/mol; **21**, ΔG_{exp} = −8.400 kcal/mol; and **24**, ΔG_{exp} = −11.910 kcal/mol), superimposed according to the DISCO-derived model, were used to develop the pseudoreceptor around the ligands. In detail, at the tips of the vectors generated by PrGen for each functional group of the ligands, residue templates were docked and oriented. When possible, amino acids were chosen on the basis of published studies on the binding site for A_1 ligands, performed by site-directed mutagenesis experiments. Otherwise, the knowledge of the primary amino acid sequence of the rat A_1 AR reported by Mahan and co-workers[51] was applied to pick up residues. Accordingly, (i) the side chain of Thr1(91) acting as a hydrogen bond acceptor was placed as the complementary counterpart to the xanthine NH. In fact, it has been reported that Thr1(91) interacts with the N^6 substituent of A_1 ligands.[3c] To grow the amino acid sequence of the pseudoreceptor, some additional residues were added to the first one. In particular, Gln2(92), Ser3(93), and Ser4-(94) were attached at the C terminus of Thr1(91), while Leu5-(90), Ile6(89), Leu7(88), Val8(87), and Pro9(86) were attached at the corresponding N terminus. (ii) The lone pair vector present on the xanthine N9 was neutralized by a hydrogen bond vector of the imidazole NH of His12(251), reported as an important residue in A_1 AR−antagonist interactions,[50b] while Ile14(252), Leu15(253), and Asn16(254) were added to the C terminus of His12(251). (iii) The carbonyl oxygen at the 2-position of **13** was involved in a hydrogen bond with the imidazole NH of His10(278), found to critically influence the binding of both agonists and antagonists to A1AR.[50b] An additional residue, Thr11(277), reported as an essential amino acid for agonist binding (interacting with the sugar portion of the ligands),[50c,63] has been added to His10(278) to fill the region of space around the N9 atom of both xanthine and adenosine A_1 antagonists. In a similar way, Ser13(281) has been placed in front of the nitrogen at the 9-position, according to the model reported by Poulsen and co-workers.[6] (iv) Hydrophobic vectors were found by PrGen, perpendicular to the adenosine or xanthine planar nucleus of the ligands, suggesting π−π interactions with the receptor. On the other hand, mutagenesis experiments on the human A_{2A} AR found that mutation of Tyr271 (conserved in the rat A_1 AR) with nonaromatic residues led to a great decrease in ligand affinity.[50a] On the basis of these findings, the adenosine or xanthine portion of the ligands was engaged in a π−π stacking interaction with Tyr17(271), while Ile18(272) and Ala19(273) (taken from the primary sequence of rat A_1 AR) were connected to its C terminus to build, together with Ile20, a wall of the cavity accommodating the C8 substituent. (v) Finally, the above-mentioned Ile20, together with Ala21, Glu22, and His23, were arbitrarily chosen and added to the growing pseudoreceptor with the aim of counterbalancing all of the remaining vectors generated by the program on the ligands, not yet saturated by the other residues. The final pseudoreceptor consisted of 23 amino acids. Next, all of the remaining ligands of the training set were inserted into the pseudoreceptor cavity to obtain the final model with embedded inhibitors.

To achieve a high correlation between experimentally derived and calculated binding energies (ΔG_{exp} vs ΔG_{calcd}), the correlation coupling protocol was applied, leading to the optimization of the pseudoreceptor, without changing position, orientation, and conformation of the ligands. In the next step, the pharmacophore was allowed to relax by minimizing the ligands without constraints while the receptor remained fixed (ligand relaxation). This allows one to remove the strain possibly imposed to the ligands by the receptor during correlation-coupled refinement but usually leads to a less highly correlated model. Therefore, correlation-coupled receptor minimization followed by unconstrained ligand relaxation was repeated until a highly correlated pseudoreceptor model was obtained in the relaxed state (designated as the equilibrated receptor). To validate the equilibrated receptor, its potency to predict free energies of binding (ΔG_{pred}) for an external set of

ligands (the test set reported in Table 2) was examined. For this purpose, the test set ligands were relaxed within the fixed equilibrated pseudoreceptor, applying the same refinement protocol as described for the training set ligands (see ligand relaxation). The linear regression obtained for the training set was used to estimate free energies of binding for the test set derivatives.[52]

In the present study, a coupling constant of 1.0 and a maximum allowed rmsd of 0.100 kcal/mol for the predicted vs experimental inhibition constants of all correlation-coupled minimization procedures were used. The target rmsd was limited to a maximum of 0.200 kcal/mol. Solvation energies of the ligands were calculated according to Still,[64] and entropy corrections were considered following Searle.[65] Compounds **13**, **16**, and **19–26** taken from the literature, characterized by A_1 AR antagonist activity ranging from 0.19 to 4300 nM, have been used in this study to build a 10 compound training set. Affinities of the investigated compounds (constituting both the training and the test set) were in part collected from the literature (compounds **13–29**) under the assumption that all of these substances are acting through the same mechanism and binding site and in part experimentally determined (compounds **10a,e,i,k** and **11h**). Taking into account the Gibbs–Helmholtz equation, conversion of experimental inhibition constants (K_i) to free energies of binding were calculated as follows: $\Delta G_{exp} = RT\ln(K_i) = 1.34$ (kcal/mol) log(K_i) at 20 °C. The complex between the pseudoreceptor and compound **13** was saved with PrGen as a pdb file and then transferred to the Viewer module of Insight II (2000) software,[66] in turn used to generate Figure 6.

Supporting Information Available: ^{1}H NMR and IR data of some representative compounds. This material is available free of charge via the Internet at http://pubs.acs.org.

References

(1) Collis, M. G.; Hourani, S. M. O. Adenosine Receptor Subtypes. *Trends Pharmacol. Sci.* **1993**, *14*, 360–366.

(2) Ralevic, V.; Burnstock, G. Receptors for Purines and Pyrimidines. *Pharmacol. Rev.* **1998**, *50*, 413–492.

(3) (a) Palczewski, K.; Kumasaka, T.; Hori, T.; Behnke, C. A.; Motoshima, H.; Fox, B. A.; Le Trong, I.; Teller, D. C.; Okada, T.; Stenkamp, R. E.; Yamamoto, M.; Miyano, M. Crystal Structure of Rhodopsin: A G Protein-Coupled Receptor. *Science* **2000**, *289*, 739–745. (b) Biancucci, A.-M.; Bigi, M.; Biagi, G.; Giorgi, I.; Livi, O.; Scartoni, V. A 3D Model of the Human A_1 Adenosine Receptor. An Evaluation of the Binding Free-Energy with Ligands. *Drug Des. Discovery* **1998**, *15*, 149–156. (c) Rivkees, S. A.; Barbhaiya, H.; IJzerman, A. P. Identification of the Adenine Binding Site of the Human A_1 Adenosine Receptor. *J. Biol. Chem.* **1999**, *274*, 3617–3621.

(4) Ji, X.-D.; von Lubitz, D.; Olah, M. E.; Stiles, G. L.; Jacobson, K. A. Species Differences in Ligand Affinity at Central A_3-Adenosine Receptors. *Drug Dev. Res.* **1994**, *33*, 51–59.

(5) Müller, C. E.; Stein, B. Adenosine Receptors Antagonists: Structures and Potential Therapeutic Applications. *Curr. Pharm. Des.* **1996**, *2*, 501–530.

(6) Poulsen, S.-A.; Quinn, R. J. Adenosine Receptors: New Opportunities for Future Drugs. *Bioorg. Med. Chem.* **1998**, *6*, 619–641.

(7) von Lubitz, D. K. J. E.; Lin, R. C. S.; Popik, P.; Carter, M. F.; Jacobson, K. A. Adenosine A3 Receptor Stimulation and Cerebral Ischemia. *Eur. J. Pharmacol.* **1994**, *263*, 59–67.

(8) Liang, B. T.; Swierkosz, T. A.; Herrmann, H. C.; Kimmel, S.; Jacobson, K. A. Adenosine and Ischemic Preconditioning. *Curr. Pharm. Des.* **1999**, *5*, 1029–1041.

(9) Müller, C. E. A_{2a} Adenosine Receptor Antagonists. Future Drugs for Parkinson's Disease? *Drugs Future* **2000**, *25*, 1043–1052.

(10) Müller, C. E. A_1 Adenosine Receptors and their Ligands: Overview and Recent Developments. *Farmaco* **2001**, *56*, 77–80.

(11) Kuroda, S.; Akahane, A.; Itani, H.; Nishimura, S.; Durkin, K.; Tenda, Y.; Sakane, K. Novel Adenosine A_1 Receptor Antagonists. Synthesis and Structure–Activity Relationships of a Novel Series of 3-(2-Cyclohexenyl-3-oxo-2,3-dyhydropyridazin-6-yl)-2-phenylpyrazolo[1,5-a]pyridines. *Bioorg. Med. Chem.* **2000**, *8*, 55–64.

(12) Suzuki, F.; Shimada, J.; Mizumoto, H.; Karasawa, A.; Kubo, K.; Nonaka, H.; Ishii, A.; Kawakita, T. Adenosine A_1 Antagonists. 2. Structure–Activity Relationships on Diuretic Activities and Protective Effects against Acute Renal Failure. *J. Med. Chem.* **1992**, *35*, 3066–3075.

(13) Nonaka, H.; Ichimura, M.; Takeda, M.; Kanda, T.; Shimada, J.; Suzuki, F.; Kase, H. KW-3902, a Selective High Affinity Antagonist for Adenosine A_1 Receptors. *Br. J. Pharmacol.* **1996**, *117*, 1645–1652.

(14) Müller, C. E. A_1 Adenosine Receptors Antagonists. *Exp. Opin. Ther. Pat.* **1997**, *7*, 419–440.

(15) Müller, C. E.; Geis, U.; Grahner, B.; Lanzner, B.; Eger, K. Chiral Pyrrolo[2,3-d]pyrimidine and Pyrimido[4,5-b]indole Derivatives: Structure–Activity Relationships of Potent, Highly Stereoselective A_1 Adenosine Receptors Antagonists. *J. Med. Chem.* **1996**, *39*, 2482–2491.

(16) Daly, J. W.; Hong, O.; Padgett, W. L.; Shamin, M. T.; Jacobson, K. A.; Ukena, D. Non-Xanthine Heterocycles: Activity as Antagonists of A_1- and A_2-Adenosine Receptors. *Biochem. Pharmacol.* **1988**, *37*, 655–664.

(17) Murphy, K. M.; Snyder, S. H. Adenosine Receptors in Rat Testes: Labeling with 3H-Cyclohexyladenosine. *Life Sci.* **1981**, *28*, 917–920.

(18) Williams, M.; Risley, E. A.; Huff, J. R. Interaction of Putative Anxiolytic Agents with Central Adenosine Receptors. *Can. J. Physiol. Pharmacol.* **1981**, *59*, 897–900.

(19) Daly, J. W.; Hutchinson, K. D.; Secunda, S. I.; Shi, D.; Padgett, W. L.; Shamin, M. T. 1-Methyl-4-substituted-1H-pyrazolo[3,4-b]pyridine-5-carboxylic Acid Derivatives: Effect of Structural Alterations on Activity at A_1 and A_2 Adenosine Receptors. *Med. Chem. Res.* **1994**, *4*, 293–306.

(20) (a) Akane, A.; Kuroda, S.; Itani, H.; Shimizu, Y. Patent NO WO9803507, 29-1-1998, CA 128:154090. (b) Akane, A.; Nishimura, S.; Kuroda, S.; Itani, H. Patent NO JP10182643, 7-7-1998, CA 129:144876.

(21) Schenone, S.; Bruno, O.; Fossa, P.; Ranise, A.; Menozzi, G.; Mosti, L.; Bondavalli, F.; Martini, C.; Trincavelli, L. Synthesis and Biological Data of 4-Amino-1-(2-chloro-2-phenylehtyl)-1H-pyrazolo[3,4-b]pyridine-5-carboxylic Acid Ethyl Ester Derivatives, a New Series of A_1-Adenosine Receptor (A_1AR) Ligands. *Bioorg. Med. Chem. Lett.* **2001**, *11*, 2529–2531.

(22) Benoit, G. Hydroxyalcoylhydrazine. *Bull. Soc. Chim. Fr.* **1939**, *6*, 708–715.

(23) Da Settimo, F.; Primofiore, G.; Taliani, S.; Marini, A. M.; La Motta, C.; Novellino, E.; Greco, G.; Lavecchia, A.; Trincavelli, L.; Martini, C. 3-Aryl[1,2,4]triazino[4,3-a]benzimidazol-4(10H)-ones: A New Class of Selective A_1 Adenosine Receptor Antagonists. *J. Med. Chem.* **2001**, *44*, 316–327.

(24) Franchetti, P.; Cappellacci, L.; Marchetti, S.; Trincavelli, L.; Martini, C.; Mazzoni, M. R.; Lucacchini, A.; Grifantini, M. 2′C-methyl Analogues of Selective Adenosine Receptor Agonists: Synthesis and Binding Studies. *J. Med. Chem.* **1998**, *41*, 1708–1715.

(25) Zbinden, P. *PrGen 2.1.1*; Biographics Laboratory: Basel, CH, 1997.

(26) Numbering of pseudoreceptor residues is given as follows. In parentheses, the amino acid sequence number taken from ref 69 is indicated. On the contrary, the number directly associated with the amino acid three letter notation is assigned automatically by PrGen. As an example, Thr1(91) is the amino acid Thr91 of the primary sequence and the residue number 1 of the PrGen labeling.

(27) van Galen, P. J. M.; Leusen, F. J. J.; Ijzerman, A. P.; Soudijn, W. Mapping the N^6 Region of the Adenosine A_1 Receptor with Computer Graphics. *Eur. J. Pharmacol. Mol. Pharmacol. Sect.* **1989**, *172*, 19–27.

(28) van der Wenden, E. M.; van Galen, P. J. M.; Ijzerman, A. P.; Soudijn, W. Mapping the Xanthine C8-Region of the Adenosine A_1 Receptor with Computer Graphics. *Eur. J. Pharmacol. Mol. Pharmacol. Sect.* **1991**, *206*, 315–323.

(29) van Galen, P. J. M.; van Vlijmen, H. W. T.; Ijzerman, A. P.; Soudijn, W. A Model for the Antagonist Binding Site on the Adenosine A_1 Receptor, Based on Steric, Electrostatic, and Hydrophobic Properties. *J. Med. Chem.* **1990**, *33*, 1708–1713.

(30) Peet, N. P.; Lentz, N. L.; Meng, E. C.; Dudley, M. W.; Ogden, A. M. L.; Demeter, D. A.; Weintraub, H. J. R.; Bey, P. A Novel Synthesis of Xanthines: Support for a New Binding Mode for Xanthines with Respect to Adenosine at Adenosine Receptors. *J. Med. Chem.* **1990**, *33*, 3127–3130.

(31) Dooley, M. J.; Quinn, R. J. The Three Binding Domain Model of Adenosine Receptors: Molecular Modeling Aspects. *J. Med. Chem.* **1992**, *35*, 211–216.

(32) van der Wenden, E. M.; Ijzerman, A. P.; Soudijn, W. A Steric and Electrostatic Comparison of Three Models for the Agonist/Antagonist Binding Site on the Adenosine A_1 Receptor. *J. Med. Chem.* **1992**, *35*, 629–635.

(33) Dooley, M. J.; Kono, M.; Suzuki, F. Conformational Search for the N6-Substituted Adenosine Analogues and Related Adenosine A1 Receptor Antagonists. *Bioorg. Med. Chem.* **1996**, *4*, 917−921.

(34) Doytchinova, I.; Petrova, S. "N6-N7"—A Modification of the "N6-C8" Model for the Binding Site on Adenosine A1 Receptors with Improved Steric and Electrostatic Fit. *Med. Chem. Res.* **1998**, *8*, 143−152.

(35) Bruns, R. F.; Fergus, J. H.; Badger, E. W.; Bristol, J. A.; Santay, L. A.; Hartman, J. D.; Hays, S. J.; Huang, C. C. Binding of the A1-Selective Adenosine Antagonist 8-Cyclopentyl-1,3-dipropyl-xanthine to Rat Brain Membranes. *Naunyn-Schmiedeberg's Arch. Pharmacol.* **1987**, *335*, 59−63.

(36) Trivedi, B. K.; Bruns, R. F. [1,2,4]Triazolo[4,3-*a*]quinoxalin-4-amines: A New Class of A1 Receptor Selective Adenosine Antagonists. *J. Med. Chem.* **1988**, *31*, 1011−1014.

(37) Ceccarelli, S.; D'Alessandro, A.; Prinzivalli, M.; Zanarella, S. Imidazo[1,2-*a*]quinoxalin-4-amines: A Novel Class of Nonxanthine A1-Adenosine Receptor Antagonists. *Eur. J. Med. Chem.* **1998**, *33*, 943−955.

(38) van Galen, P. J. M.; Nissen, P.; van Wijngaarden, I.; Ijzerman, A. P. 1*H*-Imidazo[4,5-*c*]quinolin-4-amines: Novel Non-Xanthine Adenosine Antagonists. *J. Med. Chem.* **1991**, *34*, 1202−1206.

(39) Colotta, V.; Cecchi, L.; Catarzi, D.; Filacchioni, G.; Martini, C.; Tacchi, P.; Lucacchini, A. Synthesis of Some Tricyclic Heteroaromatic Systems and their A1 and A2a Adenosine Binding Activity. *Eur. J. Med. Chem.* **1995**, *30*, 133−139.

(40) Hamilton, H. W.; Ortwine, D. F.; Worth, D. F.; Bristol, J. A. Synthesis and Structure−Activity Relationships of Pyrazolo[4,3-*d*]pyrimidin-7-ones as Adenosine Receptor Antagonists. *J. Med. Chem.* **1987**, *30*, 91−96.

(41) Thompson, R. D.; Secunda, S.; Daly, J. W.; Olsson, R. A. N6,9-Disubstituted Adenines: Potent, Selective Antagonists at the A1 Adenosine Receptor. *J. Med. Chem.* **1991**, *34*, 2877−2882.

(42) Poulsen, S.-A.; Quinn, R. J. Pyrazolo[3,4-*d*]pyrimidines: C4, C6 Substitution Leads to Adenosine A1 Receptor Selectivity. *Bioorg. Med. Chem. Lett.* **1996**, *6*, 357−360.

(43) Akahane, A.; Katayama, H.; Mitsunaga, T.; Kato, T.; Kinoshita, T.; Kita, Y.; Kusunoki, T.; Terai, T.; Yoshida, K.; Shiokawa, Y. Discovery of 6-Oxo-3-(2-phenylpyrazolo[1,5-a]pyridin-3-yl)-1(6*H*)-pyridazinebutanoic Acid (FK 838): A Novel Non-Xanthine Adenosine A1 Receptor Antagonist with Potent Diuretic Activity. *J. Med. Chem.* **1999**, *42*, 2, 779−783.

(44) Martin, Y. C.; Bures, M. G.; Dahaner, E. A.; De Lazzer, J.; Lico, I.; Pavlik, P. A. A Fast Approach to Pharmacophore Mapping and its Application to Dopaminergic and Benzodiazepine Agonists. *J. Comput.-Aided Mol. Des.* **1993**, *7*, 83−102.

(45) *AM1−MOPAC: QCPE-Program No. 455, Version 6.0*; Quantum Chemistry Program Exchange, Indiana University: Bloomington, IN.

(46) *SYBYL Version 6.5*; Tripos Inc.: St. Louis, MO, 1999.

(47) *Hint! Version 2.30S*; EduSoft, L. C.: Ashland, VA, 19.

(48) Jacobson, K. A.; Suzuki, F. Recent Developments in Selective Agonists and Antagonists Acting at Purine and Pyrimidine Receptors. *Drug Dev. Res.* **1996**, *39*, 289−300.

(49) Hess, S.; Müller, C. E.; Frobenius, W.; Reith, U.; Klotz, K.-N.; Eger, K. 7-Deazaadenines Bearing Polar Substituents: Structure−Activity Relationships of New A1 and A3 Adenosine Receptor Antagonists. *J. Med. Chem.* **2000**, *43*, 4636−4646.

(50) (a) Kim, J.; Wess, J.; van Rhee, A. M.; Schöneberg, T.; Jacobson, K. A. Site-directed Mutagenesis Identifies Residues Involved in Ligand Recognition in the Human A2a Adenosine Receptor. *J. Biol. Chem.* **1995**, *270*, 13987−13997. (b) Olah, M. E.; Ren, H.; Ostrowski, J.; Jacobson, K. A.; Stiles, G. L. Cloning, Expression, and Characterization of the Unique Bovine A1 Adenosine Receptor. *J. Biol. Chem.* **1992**, *267*, 10764−10770. (c) Townsend-

Nicholson, A.; Schofield, P. R. A Threonine Residue in the Seventh Transmembrane Domain of the Human A1 Adenosine Receptor Mediates Specific Agonist Binding. *J. Biol. Chem.* **1994**, *269*, 2373−2376.

(51) Mahan, L. C.; McVittie, L. D.; Smyk-Randall, E. M.; Nakata, H.; Monsma, F. J., Jr.; Gerfen, C. R.; Sibley, D. R. Cloning and Expressing of an A1 Adenosine Receptor from Rat Brain. *Mol. Pharmacol.* **1992**, *40*, 1−7.

(52) Zbinden, P.; Dobler, M.; Folkers, G.; Vedani, A. PrGen: Pseudoreceptor Modeling Using Receptor-Mediated Ligand Alignement and Pharmacophore Equilibration. *Quant. Struct.-Act. Relat.* **1998**, *17*, 122−130.

(53) Bassoli, A.; Merlini, L.; Morini, G.; Vedani, A. A Three-Dimensional Receptor Model for Isovanillic Sweet Derivatives. *J. Chem. Soc., Perkin Trans.* **1998**, *2*, 1449−1454.

(54) Colotta, V.; Catarzi, D.; Varano, F.; Cecchi, L.; Filacchioni, G.; Martini, C.; Trincavelli, L.; Lucacchini, A. 1,2,4-Triazolo[4,3-*a*]quinoxalin-1-one: A Versatile Tool for the Synthesis of Potent and Selective Adenosine Receptor Antagonists. *J. Med. Chem.* **2000**, *43*, 1158−1164.

(55) Pirovano, I. M.; IJzerman, A. P.; van Galen, P. J. M.; Soudijn, W. The Influence of Molecular Structure of N6-(aminoalkyl)-adenosines on Adenosine Receptor Affinity and Intrinsic Activity. *Eur. J. Pharmacol.* **1989**, *172*, 185−193.

(56) Cheng, Y. C.; Prusoff, W. H. Relation between the Inhibition Constant K_i and the Concentration of Inhibitor which Causes Fifty Percent Inhibition (IC$_{50}$) of an Enzyme Reaction. *Biochem. Pharmacol.* **1973**, *22*, 3099−3108.

(57) Ferrarini, P. L.; Mori, C.; Manera, C.; Martinelli, A.; Mori, F.; Saccomanni, G.; Barili, P. G.; Betti, L.; Giannaccini, G.; Trincavelli, L.; Lucacchini, A. A Novel Class of Highly Potent and Selective A1 Adenosine Antagonists: Structure-Affinity Profile of a Series of 1,8-Naphthyridine Derivatives. *J. Med. Chem.* **2000**, *43*, 2814−2823.

(58) Johnson, R. G.; Alvarez, R.; Salomon, Y. Determination of Adenylyl Cyclase Catalytic Activity Using Single and Double Column Procedures. *Methods Enzymol.* **1994**, *238*, 31−56.

(59) Allen, F. H.; Bellard, S.; Brice, M. D.; Cartwright, B. A.; Doubleday, A.; Higgs, H.; Hummelink, T.; Hummelink-Peters, B. G.; Kennard, O.; Motherwell, W. D. S.; Rodgers, J. R.; Watson, D. G. The Cambridge Crystallographic Data Centre: Computer-based Search, Retrieval, Analysis and Display of Information. *Acta Crystallogr.* **1979**, *B35*, 2331−2332.

(60) *MacroModel Version 5.5*; Columbia University: New York, 1996.

(61) Höltje, H. D.; Folkers, G. *Small Molecules*. In Molecular Modeling. Basic Principles and Applications; Mannhold, R., Kubinyi, H., Timmerman, H., Eds.; VCH Publishers: New York, 1996; pp 23−35.

(62) Marengo, E.; Todeschini, R. A New Algorithm for Optimal, Distance-Based Experimental Design. *Chemom. Intell. Lab. Syst.* **1992**, *16*, 37−44.

(63) Tucker, A. L.; Robeva, A. S.; Taylor, H. E.; Holeton, D.; Bockner, M.; Lynch, K. R.; Linden, J. A1 Adenosine Receptor. Two Amino Acids are Responsible for Species Differences in Ligand Recognition. *J. Biol. Chem.* **1994**, *269*, 27900−27906.

(64) Still, W. C.; Tempczyk, A.; Hawley, R. C.; Hendrickson, T. Semianalytical Treatment of Solvation for Molecular Mechanics and Dynamics. *J. Am. Chem. Soc.* **1990**, *112*, 6127−6129.

(65) Searle, M. S.; Williams, D. H. The Cost of Conformational Order: Entropy Changes in Molecular Associations. *J. Am. Chem. Soc.* **1992**, *114*, 10690−10697.

(66) *Insight II 2000*; Accelrys, Inc.: Scranton Road, San Diego, CA.

JM0209580